Carbohydrate Polymers 240 (2020) 116283

Contents lists available at ScienceDirect

Carbohydrate Polymers

journal homepage: www.elsevier.com/locate/carbpol

Nanocellulose from recycled indigo-dyed denim fabric and its application in composite films

Tuhua Zhong[a], Renuka Dhandapani[b], Dan Liang[c], Jinwu Wang[d], Michael P. Wolcott[a], Dana Van Fossen[e], Hang Liu[a,c,*]

[a] Composite Materials and Engineering Center, Washington State University, Pullman, WA 99164, USA
[b] Cotton Incorporated, Cary, NC 27513, USA
[c] Apparel, Merchandising, Design and Textiles, Washington State University, Pullman, WA 99164, USA
[d] Forest Products Laboratory, U.S. Forest Service, Madison, WI 53726, USA
[e] Department of Biomedical Engineering, Rowan University, Glassboro, NJ 08028, USA

ARTICLE INFO

Keywords:
Nanocellulose
Cotton
Indigo-dyed denim
Multifunctional
Composites

ABSTRACT

In this study, nanocellulose was extracted from indigo-dyed denim fabric and the resultant nanocellulose properties were evaluated in comparison with those derived from bleached cotton fabric and wood pulp in order to investigate the potential of recycling denim waste for nanocellulose production and application. Sulfuric acid hydrolysis and (2,2,6,6-tetramethylpiperidin-1-yl) oxyl (TEMPO)-oxidation were utilized to produce cellulose nanocrystals (CNC) and cellulose nanofibers (TOCN), respectively. A stable CNC suspension with blue color was obtained after acid hydrolysis and the TEMPO process yielded colorless TOCN. The denim-derived nanocellulose possessed similar yield, morphology, size, crystallinity, and thermal stability to those derived from bleached cotton but higher crystallinity and thermal stability compared to the nanocellulose from wood pulp. When used to reinforce polyvinyl alcohol film, the blue indigo-CNC not only enhanced mechanical properties of the film but also provided the film with outstanding UV blocking.

1. Introduction

The term nanocellulose is used broadly referring cellulose nanocrystals (CNCs) and cellulose nanofibers (CNFs) extracted from cellulose in plant cell walls (Moon, Martini, Nairn, Simonsen, & Youngblood, 2011). Nanocellulose has attracted growing attention in both academia and industry because of its attractive features such as high modulus (100 ~ 130 GPa), excellent mechanical strength with low density (1.5 ~ 1.6 g/cm^3), extremely low coefficient of thermal expansion (0.1 ppm/K), high surface area (several hundred m^2/g), unique optical properties, in addition to biocompatibility and biodegradability (Dufresne, 2013; Moon et al., 2011). Nanocellulose can be used in paper packaging, coatings, automotive parts, cosmetics, composites, biomedical devices, energy storage, water purification, *etc.*(Brinchi, Cotana, Fortunati, & Kenny, 2013; Hamad, 2006; Reid, Villalobos, & Cranston, 2017).

CNCs are usually isolated from semi-crystalline cellulose fibers using a traditional strong acid hydrolysis process in which the amorphous region is digested with the crystalline region intact and thus individual crystallites are released with the assistance of mechanical disintegration processes (*e.g.*, ultrasonication) (Habibi, Lucia, & Rojas, 2010). Sulfuric acid is one of the most commonly used inorganic acids because of its low cost and also because that sulfuric acid can react with the hydroxyl groups on the surface of crystallites to introduce anionic sulfate half-ester groups. These negatively charged groups play an important role in stabilizing CNCs in water (Habibi et al., 2010; Rebouillat & Pla, 2013). CNFs can be extracted through (2,2,6,6-tetramethylpiperidin-1-yl) oxyl (TEMPO)-oxidation pretreatment followed by mechanical disintegration. The TEMPO oxidation method is regarded as an effective and efficient way to produce CNFs because primary hydroxyl groups are regioselectively converted into anionic carboxylate groups ($-COO^-$) under alkaline conditions. The negative charges induce interfibrillar electrostatic repulsion forces and thereby facilitate nanofibrillation in the subsequent mechanical separation process (Isogai, Saito, & Fukuzumi, 2011; Saito & Isogai, 2004).

Nanocellulose can be extracted from a wide range of sources, such as wood, cotton, ramie, sisal, flax, tunicate, and algae (Beck-Candanedo, Roman, & Gray, 2005). To date, wood has been the main source because of its abundance in nature. Most of the industrially produced nanocellulose comes from wood pulp, especially from bleached Kraft wood pulp (de Assis et al., 2017). While wood pulp

* Corresponding author at: Apparel, Merchandising, Design and Textiles, Washington State University, Pullman, WA 99164, USA.
E-mail address: hangliu@wsu.edu (H. Liu).

https://doi.org/10.1016/j.carbpol.2020.116283
Received 5 February 2020; Received in revised form 7 April 2020; Accepted 9 April 2020
Available online 17 April 2020
0144-8617/

remains a leading source for nanocellulose, material such as the by-products of agricultural crops and cellulose waste is highly desired for reduced raw material cost. Currently, extracting cellulose nanocrystals from two post-process agro-industrial by-products, cotton gin motes and cotton gin waste, has been reported (Jordan, Easson, Dien, Thompson, & Condon, 2019). Cotton is the purest form of cellulose in nature and the cellulose content is usually more than 90 % in raw cotton fibers in comparison with 40 ~ 50 % in wood (Dufresne, 2013; Wang, Yao, Zhou, & Zhang, 2017). Cotton is the major fiber for apparel and home textiles. In finished cotton fabrics, cellulose content can be up to 99 % because non-cellulose components are eliminated during scouring and bleaching, which are routine preparation procedures. Consumption of cotton products has been steadily growing over the past decades. It was reported that approximately 110 and 115 million bales of cotton were consumed globally in 2016 and 2017, respectively (Liu et al., 2019; Wang et al., 2017). These convert to approximately 25 and 26 billion kilograms of cotton fibers. As a result of the increased consumption, the amount of cotton waste generated, including both pre-consumer (fiber linters, yarn slivers, fabric scraps from factory offcuts, unsold brand new garments) and post-consumer (used and unwanted garments) waste, is substantial (Liu et al., 2019). Denim jeans are very popular clothing among consumers and they are made from fabrics usually containing 95–100 % cotton fibers. It is estimated that around five billion square meters of indigo-dyed denim fabrics are produced every year (Bechtold, Maier, & Schrott, 2005; Maryan & Montazer, 2013). Due to the lack of efficient recycling techniques, most denim garments at the end of their service life are thrown away and end up in landfills or incinerators. This not only is a huge loss of excellent cellulose resources but also poses environmental issues as a result of cotton anaerobic degradation and burning. Moreover, indigo dyes are released into soil because they are very difficult to decompose biologically (Wambuguh & Chianelli, 2008). With natural materials become rarer and the awareness of environment protection increases, it is imperative to develop methods to recycling denim waste for the closed-loop sustainable development. Currently, the major cotton recycling method is fiber reclamation via shredding for building/automotive insulation materials, furniture, and yarn spinning for lower quality products (Liu et al., 2019). This is considered a downgrade recycling because the fibers reclaimed do not have enough strength/elasticity for high-quality products, ascribing to the many mechanical stresses that fibers are subject to during the process, including tension, compression, bending, and twisting (EI Mogahzy, 2009; Haule, Carr, & Rigout, 2016). When the stresses exceed their elastic limit, fibers are permanently deformed or broken. In contrast to mechanical reprocessing at the macroscale which causes strength loss of the recycled fibers, extracting cellulose at the nanoscale can remove most of the defects linking the hierarchical structure and produce ideal cellulose-based nano “building blocking” for a wide range of high value-added applications, particularly in composite reinforcement (Haule et al., 2016; Moon et al., 2011). The use of cotton wastes as a raw material for the generation of nanocellulose might be a promising solution to recycle cotton-sourced materials. Several studies have reported the extraction of nanocellulose from cotton stalks, cotton slivers, fibers, linters, and fabrics (Morais, de Freitas Rosa, Nascimento, do Nascimento, & Cassales, 2013; Shamskar, Heidari, & Rashidi, 2016; Soni & Mahmoud, 2015; Teixeira et al., 2016; Wang et al., 2017). So far, no published research has been found on producing nanocellulose from indigo-dyed post-consumer denim and studying the impact of indigo on the extraction process and the properties of nanocellulose produced.

In this study, indigo-dyed denim fabric was selected as the starting material for nanocellulose production using both sulfuric acid hydrolysis and TEMPO oxidation methods. Nanocellulose produced from bleached cotton fabric and wood pulp was used for comparison purpose. The influence of indigo dyes on the extraction of nanocellulose and the material properties of the resulting nanocellulose was investigated. Properties such as nanocellulose yield, morphology, size, surface charges, crystallinity, and thermal stability were determined. In addition, the nanocellulose thus derived in this study was tested as a reinforcing material in polyvinyl alcohol (PVA) composite films. The tensile properties and light transmission of PVA composites were evaluated.

2. Material and methods

2.1. Materials

Bleached cotton fabric and indigo-dyed fabric were kindly provided by Cotton Incorporated (North Carolina, USA). Northern Softwood Bleached Kraft Pulp in sheet was from the U.S. Department of Commerce National Institute of Standards and Technology. Sulfuric acid (H_2SO_4, 95.7 wt%, Certified ACS Plus) was from Fisher Scientific. Sodium hypochlorite solution (NaClO, 10–15 %, reagent grade), 2,2,6,6-tetramethylpiperidine 1-oxyl (TEMPO, crystal), Sodium bromide (NaBr, crystal, ACS) were from Sigma-Aldrich. Sodium hydroxide (NaOH, pellets, certified ACS) and hydrochloric acid (HCl, 36.5–38.0 wt %, certified ACS) were from Fisher Chemical. Ethanol (200 proof, anhydrous) was from Decon Labs, Inc. Poly (vinyl alcohol) (PVA, 88 % hydrolyzed, average M.W. 88000) was from Acros Organics.

2.2. Size reduction pretreatment of denim and bleached cotton fabrics

Bleached white cotton fabric and indigo-dyed denim fabric were ground to approximately 2 mm long using a Contra Selector Mill (Pallmann, Germany). Wood pulp sheets were cut to pieces by a Mini Wiley Mill (Thomas Scientific, USA).

2.3. Cellulose nanocrystals production via sulfuric acid hydrolysis approach

Ground cotton fibers (4 g) were mixed with sulfuric acid (70 mL) at a 64 wt% concentration for acid hydrolysis at 45 ℃ for 1 h. The reaction was then stopped by adding 10-fold distilled water to the mixture. The hydrolyzed cellulose was washed by centrifuge and then dialyzed against water for ~5 days, and finally were further disintegrated via intense ultrasonication (Branson Ultrasonics, USA) for 10 min to obtain well-dispersed CNC suspensions. The resulting cellulose nanocrystals from bleached cotton fabric and indigo-dyed denim were coded as CNC(bleached cotton) and CNC(indigo-dyed denim), respectively. The CNC suspensions were stored at 4 ℃ before use and characterization. The same acid hydrolysis condition was applied to shredded wood pulp to obtain CNC from wood pulp and was labeled as CNC(wood pulp).

2.4. Cellulose nanofibers production via TEMPO-mediated oxidation approach

Ground cotton fibers (4 g) were suspended in water (400 mL) to be swollen overnight. TEMPO (0.064 g) and sodium bromide (0.4 g) were then added to the suspension. The oxidation of the cotton was initiated by adding the solution of NaClO (23 g) to the mixture. The pH of the reaction mixture was maintained at 10.0 ~ 10.5 by adding 0.5 M NaOH solution. The reaction continued at room temperature for 6.5 h. Upon the define reaction time, the ethanol (8 mL) was added to stop the reaction. The pH was then adjusted to 7.0 with 0.5 M HCl. The TEMPO-oxidized cellulose (TOC) was washed by centrifuging and then dialyzed against water for ~5 days. Mechanical disintegration of the TOC was carried out with a microfluidizer (LM20, microfluidics, USA). The TOC suspensions were passed through the interaction chambers five times under the pressure of 30,000 psi to generate a dispersion of TEMPO-oxidized cellulose nanofibers (TOCN). The resulting cellulose nanofibers were coded as TOCN(bleached cotton) and TOCN(indigo-dyed denim) from the bleached cotton fabric and indigo-dyed denim, respectively. The TOCN suspensions were stored at 4 ℃ before use and characterization. The same TEMPO oxidation condition was applied to

the shredded wood pulp and the obtained TOCN was labeled as TOCN (wood pulp).

2.5. PVA/nanocellulose film fabrication

The nanocellulose suspensions were adjusted to predefined consistency and PVA was added for dissolving at 90 ℃ under magnetic stirring for 1.5 h. After centrifuging degas, the blended PVA/nanocellulose suspensions were cast into a mold and were dried at 40 ℃ for 72 h to obtain films. According to the weight ratio of nanocellulose in the films (*i.e.*, 0, 5, and 10 %), the types of nanocellulose (*i.e.*, CNC and TOCN), and the starting materials (*i.e.*, bleached cotton fabric and indigo-dyed denim fabric), the resultant nanocomposite films were labeled as PVA, PVA/CNC(cotton)5, PVA/CNC(cotton)10, PVA/CNC(denim)5, PVA/CNC(denim)10, PVA/TOCN(cotton)5, PVA/TOCN(cotton)10, PVA/TOCN(denim)5, and PVA/TOCN(denim)10.

2.6. Material characterizations

2.6.1. Scanning electron microscopy (SEM) observation

Surface morphology of the shredded bleached cotton, indigo-dyed denim and wood pulp was observed with a scanning electron microscope (SEM, Quanta 200 F, FEI, USA) at a voltage of 20 kV. Prior to the SEM observation, the samples were coated with platinum with a sputtering process.

2.6.2. Transmission electron microscopy (TEM) observation

Morphology of CNC and TOCN observation was performed with a transmission electron microscopy (TEM, Tecnai G2 20 Twin, FEI, USA) at an accelerating voltage of 200 kV. Prior to observation, the diluted CNC and TOCN dispersions were deposited on a Formvar/carbon-coated copper grid, then were stained by 2% uranyl acetate, and were finally dried overnight.

2.6.3. Zeta potentials measurement

The zeta potentials of the nanocellulose suspensions with 10 mM sodium chloride (NaCl) added were measured with a Zetasizer-Nano (Malvern, UK) at a consistency of ~ 0.1 wt% and a pH of 7. The measurements were performed in triplicate.

2.6.4. Surface charge density measurement by conductometric titration

The sulfate half-ester content on the CNC surface was measured by conductometric titration as described in Foster et al. (2018) and Jordan et al. (2019). In brief, 5 ~ 10 g acid-form ($^{-}$ OSO_3H) CNC suspensions (0.5 ~ 1.0 wt%) was diluted to a volume of 99 mL by adding water, and then 1 mL of 100 mM sodium chloride (NaCl) solution was added to increase the conductivity to a measurable range. Under constant stirring, 100- μ L aliquots of 100 mM NaOH solution was added at intervals. Following each NaOH addition, stabilizing the conductivity for at least 30 s was allowed before recording the value. The molar surface charge (mmol/g of CNC) was determined graphically by plotting the volume-corrected conductivity of the CNC suspension as a function of the volume of NaOH added. The equivalent molar surface charge was calculated via the molar volume of NaOH added, which was determined by the intersection point of the linear-regressions of the regions before and after the equivalence point. The volume-corrected conductivity was calculated using the following equation:

$$Conductivity_c = Conductivity_m \times \left(\frac{V_i + V_0}{V_0}\right)$$

where $Conductivity_c$ was the corrected conductivity (μ s/cm); $Conductivity_m$ was the measured conductivity for each data point (μ s/cm); V_i was the initial suspension volume (mL) prior to the addition of the first 100- μ L aliquotes of 100 mM NaOH solution; and V_0 was the added volume of NaOH at each point (mL).

The carboxylate content of TOCN was determined by conductometric titration as briefly described here. 5 ~ 10 g TOCN suspensions (0.5 ~ 1.0 wt%) was diluted to a volume of 99 mL by adding water, and then 1 mL of 100 mM hydrochloride acid (HCl) solution was added to ensure full protonation of the weak acid. Titrations were conducted as described for the CNC samples. The volume-corrected conductivity was plotted as a function of the volume of NaOH added, and the equivalence point was determined by the intersection of the plateau formed between the linear regressions from the strong acid equivalence point and weak acid equivalence point. The molar surface charge (mmol/g of TOCN) was calculated as the molar volume of NaOH added between the strong acid and the weak acid equivalence points. The conductometric titration measurements were performed in triplicate.

2.6.5. X-ray diffraction (XRD) measurement

The diffractograms of freeze-dried nanocellulose were measured using an X-ray diffractometer (Rigaku Miniflex 600, Japan) with a Cu Kα X-ray source (λ = 0.1548 nm) at 40 kV and 15 mA. The crystallinity index (CrI) was calculated using an equation as described by Segal, Creely, Martin, and Conrad (1959). $CrI = (I_{002} - I_{amorphous})/ I_{002}$, where I_{002} is the intensity of the main peak (002) and $I_{amorphous}$ is the intensity of the amorphous portion at 2θ = 18.0 °.

2.6.6. Fourier-transform infrared (FTIR) analysis

Infrared spectra of the shredded bleached cotton, shredded indigo-dyed denim, shredded wood pulp, and the freeze-dried CNC and TOCN products were measured using Fourier-transform infrared spectroscopy (FTIR, Nicolet iS-50, Thermal Fisher Scientific, USA) with a resolution of 4 cm^{-1} and 64 scans under the absorbance mode. Prior to FTIR analysis, thin pellets comprising the samples and potassium bromide (1/50, %W/W) were prepared.

2.6.7. Thermal property analysis

The thermal properties of raw materials and the freeze-dried nanocellulose and a series of the PVA/nanocellulose composite films were tested by a thermogravimetric analyzer (STAR^e system, Mettler Toledo, Switzerland) at a heating rate of 10 ℃/min and a nitrogen purging flow rate of 100 mL/min.

2.6.8. Tensile test

Tensile strength and modulus of the PVA/nanocellulose films (length × width × thickness = 60 mm × 10 mm × 0.06 mm) were evaluated with an Instron Material Testing Machine (Model 4466, Instron, USA) in accordance with ASTM standard D638-14. The initial distance between the grips was 25 mm, and the separation rate of the grips was kept constant at 25 mm/min. Ten test specimens for each sample were tested and the average was reported.

2.6.9. Water contact angle measurement

The water contact angles of the CNC films extracted from indigo-dyed denim and bleached cotton were measured with a VCA Optima Video Contact Angle System (AST products Co., USA). CNC films were obtained by solvent-casting of CNC suspensions and were air-dried.The water contact angles were recorded after the water droplet immediately contacted (at 0.2 s) the CNC film surface. The measurements were performed in triplicate at room temperature.

2.6.10. Differential scanning calorimetry (DSC) measurement

The thermal transitions of the PVA/nanocellulose composites were examined by a DSC system (STAR^e system, Mettler Toledo, Switzerland) with a nitrogen flow rate of 100 mL and with a cooling system. Sample (~ 5 g) was sealed in an aluminum crucible and heated from $^{-}$ 20 ℃ to 250 ℃ at a heating rate of 10 ℃ /min (first heating scan), and then cooled at 10 ℃ /min from 250 ℃to $^{-}$ 20 ℃ (first cooling scan) followed by heating again to 250 ℃ at 10 ℃ /min (second heating scan). The first

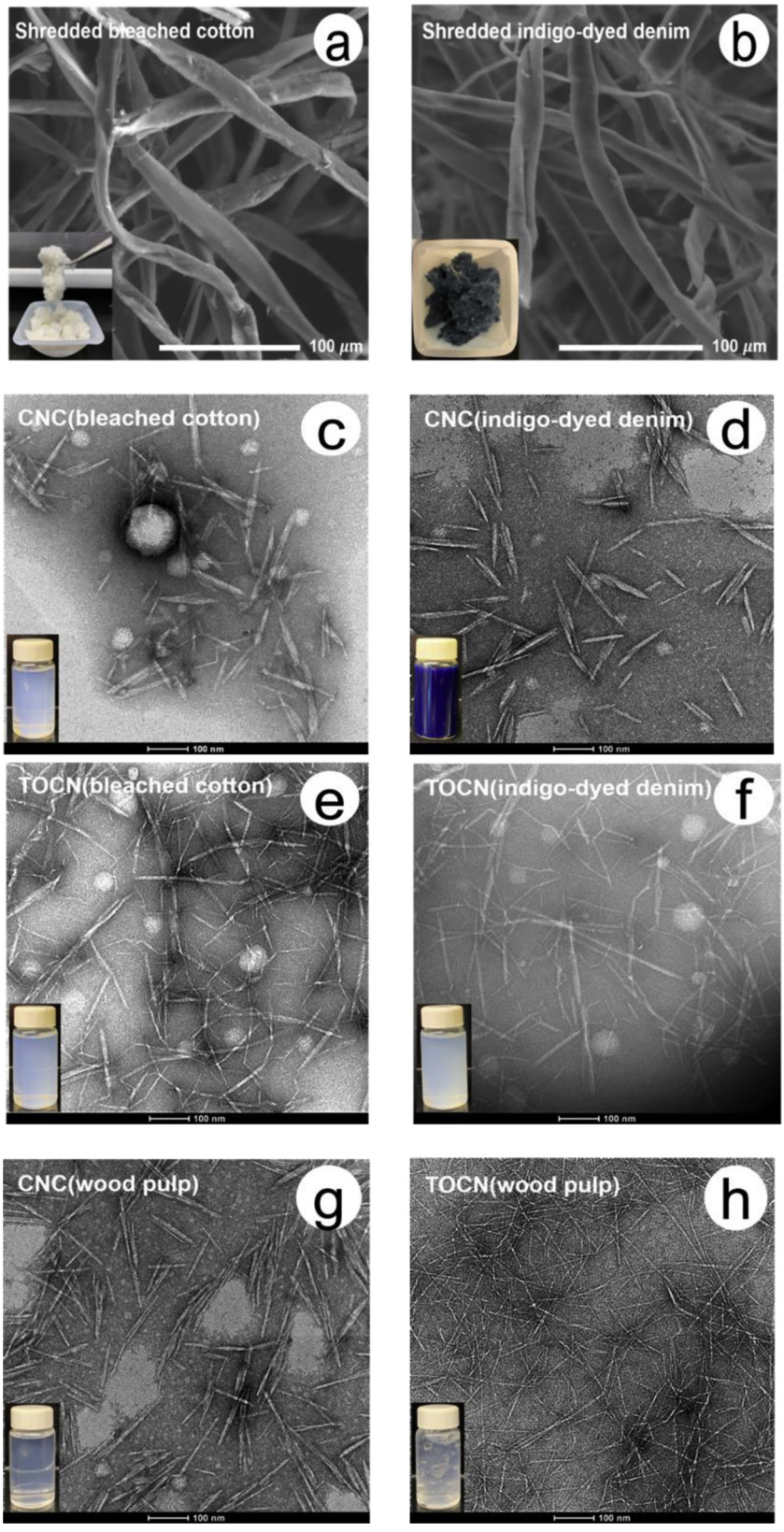

Fig. 1. SEM images of (a) shredded bleached cotton and (b) shredded indigo-dyed denim (inset: photos of the respective shredded fabrics); TEM images of (c) CNC(bleached cotton), (d) CNC(denim), (e) TOCN(bleached cotton), and (f) TOCN(denim), (g) CNC(wood pulp), and (h) TOCN(wood pulp) (inset: photos of the respective nanocellulose suspensions).

Table 1
Comparison of material properties of nanocellulose obtained from indigo-dyed denim with those obtained from bleached cotton and wood pulp.

Sample	Size		Zeta potential (mV)	Surface charge density (mmol/g)	Crystallinity index (%)	Yield (%)
	Width (nm)	Length (nm)				
Shredded bleached cotton	13.4±4.4 (μm)	—	—	—	78.1	—
Shredded indigo-dyed denim	15.3±3.7 (μm)	—	—	—	68.0	—
Shredded wood pulp	22.6±6.8 (μm)	—	—	—	59.9	—
CNC(bleached cotton)	11.9±6.7	127.7±43.8	−33±2	0.28±0.01	86.4	39.6
CNC(indigo-dyed denim)	12.5±4.3	151.7±52.6	−36±2	——	85.6	37.8
CNC(wood pulp)	8.1±2.5	198.7±64.2	−52±3	0.56±0.05	77.9	8.9
TOCN(bleached cotton)	11.4±5.3	175.2±93.0	−52±2	1.59±0.06	71.6	72.6
TOCN(indigo-dyed denim)	9.90±3.8	162.3±86.0	−52±3	1.64±0.08	66.0	78.9
TOCN(wood pulp)	4.8±1.7	264.9±71.8	−54±4	1.69±0.13	48.9	82.8

heating scan was performed to eliminate the samples' thermal history.

2.6.11. Ultraviolet-visible (UV–vis) analysis

The light transmittance of the PVA/nanocellulose nanocomposite films was measured with a UV–vis spectrophotometer with a scan from 200 nm to 800 nm (Lambda-25, PerkinElmer, USA).

3. Results and discussion

3.1. Characteristics of the resulting nanocellulose

Fig. 1 shows the morphology of the cotton fibers ground from bleached and denim fabrics under SEM, and the produced CNC and TOCN under TEM. Table 1. contains information about the size, zeta potential (ZP), surface charge density, crystallinity index (CrI), and nanocellulose yield of CNC and TOCN, as well as the size and crystallinity of the original cotton and wood pulp. The shapes of CNC and TOCN from cotton fibers were similar to those from wood pulp, *i.e.*, CNC was rod-like and TOCN was fibril-like. In terms of size, the widths of both CNC and TOCN from cotton were wider and the lengths were shorter than those from wood pulp. This might indicate that the microfibrils in cotton were larger in size and comprised more cellulose chains than those in wood pulp. TEMPO oxidation produced relatively long nanofibers with a higher degree of entanglement, especially TOCN (wood pulp), as can be seen in Fig. 1. There was no significant size difference between the nanocellulose from the bleached cotton and that from indigo-dyed denim. When compared to the nanocellulose reported in the literature, it was found that the size of the CNC from wood pulp produced in this study was similar to those reported by others. According to Reid et al. (2017), commercially available and lab-made wood-sourced CNC usually has a diameter of 6–8 nm and a length of 130–190 nm when manufactured with 63.5 ~ 64 wt% sulfuric acid at 45 ℃ for 45 min to 2 h.

The crystallinity indexes of the original cotton fibers and the extracted nanocellulose, both CNC and TOCN, were higher than those from wood pulp. Compared to the original cotton, the crystallinity of CNC was higher and that of TOCN was lower. The crystallinity of CNC from the cotton fibers was the highest at approximately 86 %. This was because the cellulose amorphous regions were preferentially hydrolyzed and degraded into soluble products during sulfuric acid hydrolysis, while the crystalline domains mostly remained intact due to their high ordered molecular chain arrangement that resisted acid penetration (Habibi et al., 2010). For the same reason, it was expected that the CNC yield would be lower than the TOCN yield as the results shown in Table 1. The CNC yield from the cotton fibers was about half of the TOCN yield. The CNC yield from the wood pulp was only 8.9 % under the acid hydrolysis condition used in this study (64 wt% sulfuric acid at 45 ℃ for 60 min), which was significantly lower than the CNC yield from both bleached and denim cotton fibers. This indicates that cotton-sourced cellulose is more resistant to acid attack than wood-sourced cellulose. The higher crystallinity, larger degree of polymerization, and likely the larger crystallite size of cotton fibers are possible reasons. Reducing acid hydrolysis time of wood pulp from 60 min to 25 min brought up the yield from 8.9%–31.4% because the shortened hydrolysis duration alleviated cellulose degradation and avoided the peel off of cellulose sheets from the crystalline region (Helbert, Nishiyama, Okano, & Sugiyama, 1998). This was consistent to what previous studies had found that the characteristics (size, surface charge density, crystallinity, and yield) of CNCs are highly dependent on the nature of the cellulose source, the acid used and its concentration, acid-to-cellulose ratio, reaction temperature, reaction time, *etc.* (Beck-Candanedo et al., 2005; Dong, Revol, & Gray, 1998; Reid et al., 2017).

CNC obtained from cotton fibers was also reported by other researchers. Sulfuric acid hydrolysis of Whatman No. 1 filter paper powder (98 % cotton fibers) using 64 wt% acid concentration and 8.75 mL/g acid-to-cellulose ratio at 45 ℃ for 1 h produced CNC with a diameter of 7 nm and a length of 197 nm (Dong et al., 1998). The yield was 44 %. The obtained CNC from shredded cotton fabrics in this study had slightly lower yield, shorter length but larger diameter. TOCN manufactured using the TEMPO oxidation method from never-dried cotton and never-dried sulfite pulp by Saito, Nishiyama, Putaux, Vignon, and Isogai (2006) had a regular width of 3 ~ 5 nm. In this study, the TOCN derived from softwood bleached Kraft pulp exhibited a similar size (~ 5 nm) in diameter, but the diameter of the TOCN obtained from cotton fabrics were much larger (10 ~ 12 nm).

The insets in Fig. 1c-g are photographs of nanocellulose suspensions. Interestingly, the CNC suspension obtained from denim had dark blue color (Fig. 1d) while all the other suspensions were clear without color, including the TOCN from denim. It is clear that the indigo dyes were not degraded by the strong acid hydrolysis and they co-existed in the suspension with CNC in a stable state. The dialysis washing process did not remove the small indigo dye molecules. In contrast, transparent TOCN suspension was obtained from denim showing that the TEMPO-mediated oxidation process oxidized cellulose and simultaneously degraded indigo dyes in the TEMPO/NaClO/NaBr system (Bechtold et al., 2005). During the oxidation process, the color of the fiber suspension changed from dark blue, to light blue, and light green till colorless.

The zeta potential and the surface charge density are summarized in Table 1. No reliable surface charge density of CNCs from indigo-dyed denim was obtained in this study and this was possibly due to the interference of indigo dyes in the suspension. The electrostatic repulsion force due to the negative charges of the anionic groups on the nanocellulose surface allowed to facilitate nanofibril separation during extraction and promote the stable dispersion in water/solvents. For TOCN, the negative charges are from anionic carboxylate groups ($^{-}COO^{-}$), which are converted from primary hydroxyl groups at the surface of nanocellulose (Isogai et al., 2011; Saito & Isogai, 2004). The negative charges of CNC are attributable to the sulfate half-esters ($^{-}OSO_3^{-}$) resulted from the esterification reaction of sulfuric acid and hydroxyl. Results from this study showed that the ZPs of nanocellulose (both CNC and TOCN) from wood pulp were higher than those from cotton fibers, respectively. This was consistent with the smaller widths

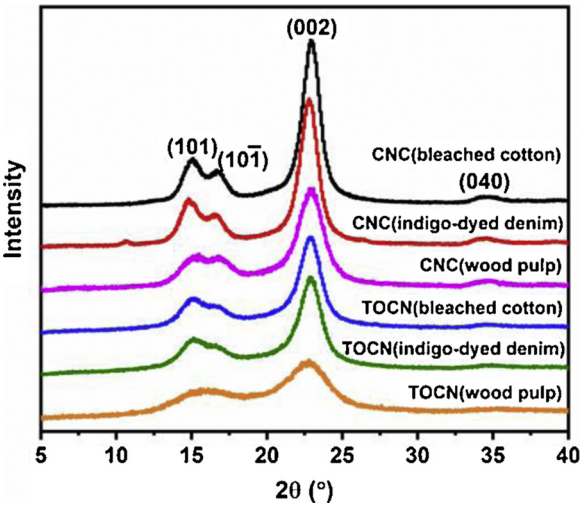

Fig. 2. XRD patterns of CNC and TOCN from bleached cotton, indigo-dyed denim, and wood pulp.

of CNC and TOCN from wood pulp compared to those from cotton fabrics. The CNC derived from the denim fabric had similar zeta potential to those from the bleached cotton fabric, but was lower than that of CNC from wood pulp. The ZP and the surface charge density were similar for all the TOCN extracted from different sources.

Fig. 2 shows XRD patterns of nanocellulose from different sources. Four characteristic peaks were observed at 2 θ of 15.0 °, 16.8 °, 22.9 °, and 34.4 ° corresponding to the (101), (10$\bar{1}$), (002), and (040) reflection planes, respectively (Hamad & Hu, 2010; Wada, Heux, & Sugiyama, 2004). These diffraction peaks indicated the crystal structure in all the nanocellulose was cellulose I β type, the dominant polymorph in the cell wall of higher plants (French & Cintrón, 2013; French, 2014; Moon et al., 2011). The peaks are more evident in the CNC products than in the TOCNs. Sharper diffraction patterns (Fig. 2) were good indications of a higher degree of crystallinity, as evidenced in Table 1. The densely packed molecules in crystalline regions can provide strength, swelling resistance and thermal stability to cellulose fibers (Pedersoli Júnior, 2000). Having higher cellulose crystallinity makes the nanocellulose more attractive as a reinforcing material in composite applications.

3.2. FTIR analysis

The infrared spectra of CNC and TOCN products are displayed in Fig. 3. As shown in the close-up spectra in Fig. 3b, the intensity of the absorbance band at around 1034 cm^{-1} in the CNC products significantly increased compared to their respective raw starting materials and the TOCN products. This was likely due to the refinement of the cellulose crystal structure, which resulted in distinct vibration mode. Another possible explanation for this increased intensity of the band at 1034 cm^{-1} might be ascribed to the introduction of the sulfate groups. Lin and Dufresne (2014) found that the intensity of the band at 1033 cm^{-1} was increased due to the increased sulfate groups by surface post-sulfation treatment while the intensity was reduced after surface de-sulfation treatment. The introduction of sulfate groups on the CNC might partially account for the increased intensity of the band at 1034 cm^{-1} in addition to the refinement of the cellulose crystal structure. A weak band observed at around 1650 cm^{-1} was ascribed to the adsorbed water in cellulose (Foster et al., 2018). After the TEMPO oxidation, a new band occurred at around 1620 cm^{-1}, which overlapped with the band at around 1650 cm^{-1}, was due to the C = O stretching vibration of carboxylate groups ($^-$ COO$^-$) on TOCN (Fukuzumi, Saito, Okita, & Isogai, 2010). Three characteristic bands of indigo dyes at around 1631 cm^{-1}, 1615 cm^{-1}, 1482 cm^{-1} were only observed in the spectra of the original denim and its derived CNC but not those of bleached cotton, its derived CNC, and TOCN (indigo-dyed denim). These three bands were resulted from the stretching vibration of the C = O, the C = C stretching vibration of the aromatic ring, and the C $^-$ H rocking vibration on indigo molecules, respectively (Baran, Fiedler, Schulz, & Baranska, 2010; Lakshmi, Srivastava, Mall, & Lataye, 2009; Ortiz et al., 2016). This result further indicated that the indigo dye had been degraded in the TEMPO oxidation process, there was negligible, or no indigo dye left on the TOCN products.

3.3. Thermal property analysis of nanocellulose

Fig. 4 displays the thermogravimetric analysis (TGA) and derivative thermogravimetric (DTG) curves of the starting materials, CNC, and TOCN products. Temperatures of onset degradation, at 5% and 50 % weight loss, and maximum degradation are listed in Table 2. The original bleached cotton and indigo-dyed denim exhibited two weight loss stages. The first stage occurred at around 50 ~ 150 ℃due to the loss of absorbed water and residual moisture in the products, and the second stage was observed at approximately between 325 and 400 ℃ corresponding to the thermal degradation of cellulose, *i.e.,* depolymerization, dehydration, and decomposition of glycosyl units to form solid char eventually (Roman & Winter, 2004). The original indigo-dyed denim exhibited less thermal stability than bleached cotton with lower degradation temperatures, especially at the beginning degradation stage. For CNCs in sodium form, the maximum decomposition corresponding to the degradation of the cellulose backbone occurred at around 325 ℃and 340 ℃ for CNCs from the bleached and indigo-dyed denim fabrics, respectively, compared to 362 ℃ and 350 ℃of their starting materials. CNC in sodium form had much higher thermal stability than that of CNC in acid form, as shown in Table S1; the result was consistent to the result reported by others (Vanderfleet et al., 2019). A shoulder

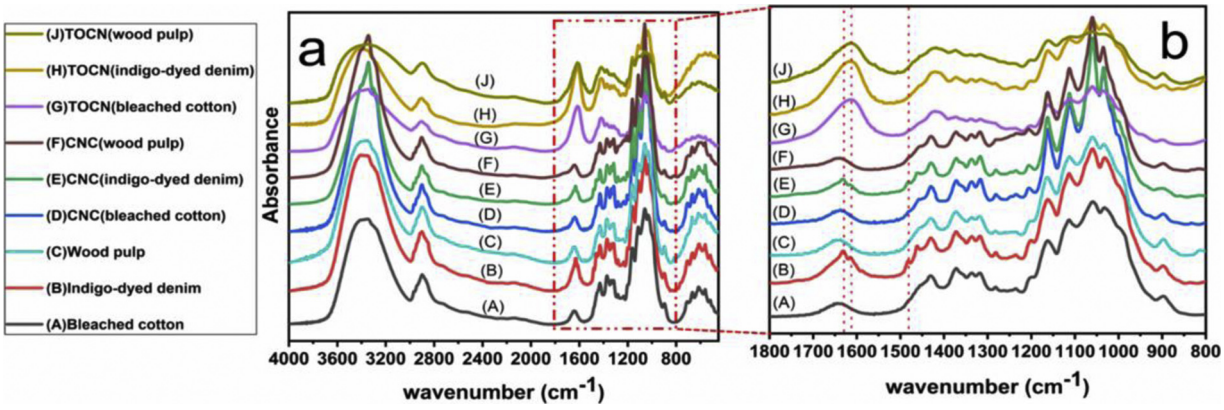

Fig. 3. (a) FTIR spectra of shredded cotton materials, CNC and TOCN products; (b) the close-up spectra at the selected wavenumber range.

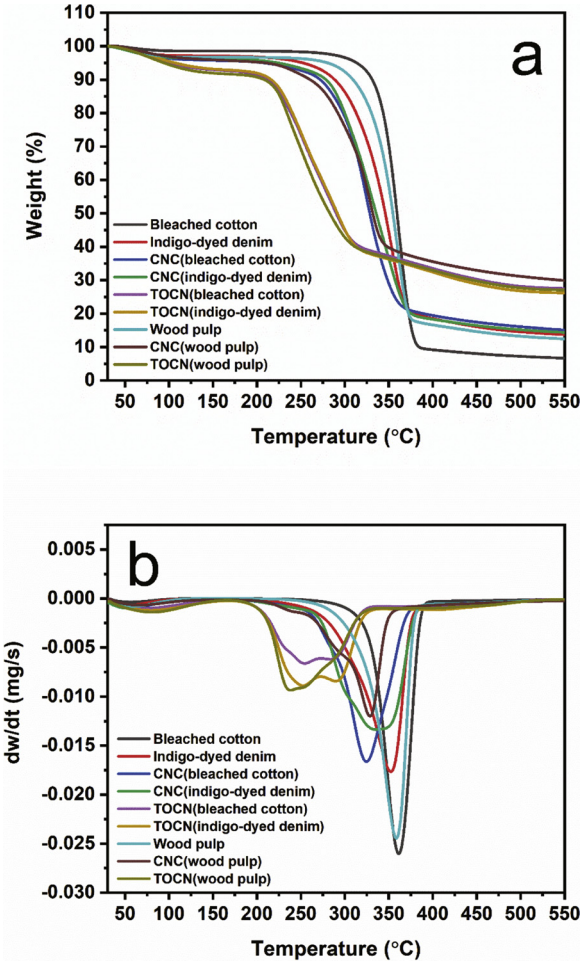

Fig. 4. Typical TGA curves (a) and DTG curves (b) of the starting materials, the obtained CNC and TOCN products.

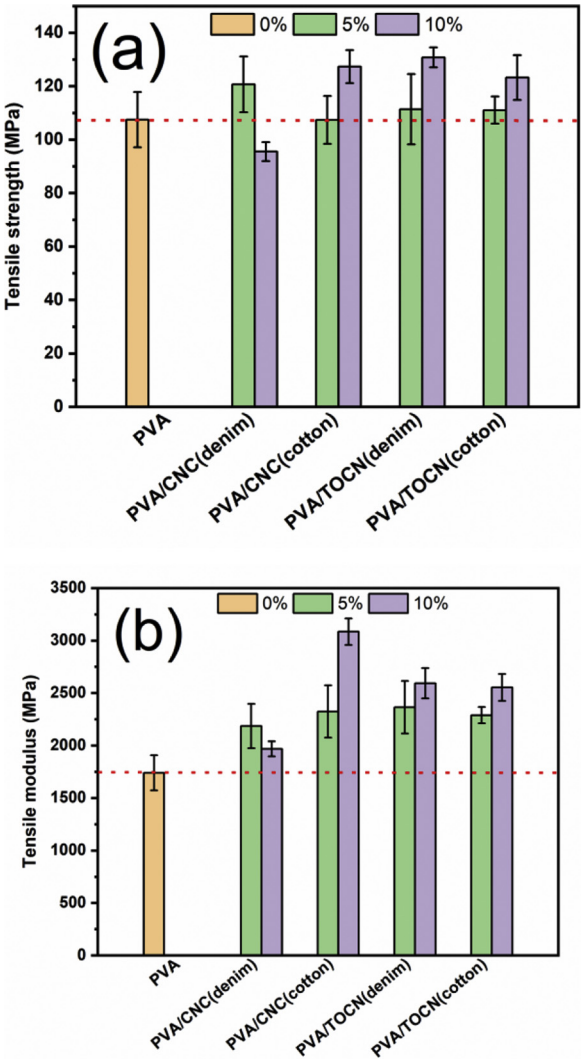

Fig. 5. Tensile strength (a) and tensile modulus (b) of the PVA composites with different types of nanocellulose at various concentrations (0%, 5%, and 10 %).

appeared at around 250 °C in DTG curves of CNCs from both bleached cotton and denim attributing to the decomposition of sulfate half-esters on the cellulose surface. During pyrolysis, these sulfate groups were released at around 250 °C and then functioned as a dehydration catalyst, which resulted in lower thermal stability of the CNCs (Jiang & Hsieh, 2015; Kim, Nishiyama, Wada, & Kuga, 2001; Lin & Dufresne, 2014). Similarly, a small number of finishing chemicals in the denim fabric might have catalyzed its degradation and resulted in its lower thermal stability than that of the bleached cotton. During CNC extraction, the chemical might have been removed so the difference between the CNCs derived from the bleached cotton and the CNCs derived from the indigo-dyed denim was smaller.

TOCNs derived from the indigo-dyed denim exhibited similar thermal behavior in comparison to that from the bleached cotton. Both had DTG curves consisting of two main decomposition temperature

Table 2
Degradation temperatures for nanocellulose obtained from different sources.

Sample	Onset degradation temperature (°C)	$T_{5\%}$[a] (TGA curves) (°C)	$T_{50\%}$[b] (TGA curves) (°C)	Max degradation temperature (DTG curves) (°C)	
				T_{peak1}	T_{peak2}
Shredded bleached cotton	340	314	359	362	
Shredded indigo-dyed denim	300	252	346	350	
Shredded wood pulp	320	277	351	355	
CNC(bleached cotton)[c]	275	208	328	325	
CNC(indigo-dyed denim)[c]	285	224	336	340	
CNC(wood pulp)[c]	260	210	332	328	
TOCN(bleached cotton)[d]	229	100	290	255	280
TOCN(indigo-dyed denim)[d]	230	107	291	250	290
TOCN(wood pulp)[d]	225	94	283	230	250

[a]Degradation temperature corresponding to 5% weight loss.
[b]Degradation temperature corresponding to 50 % weight loss.
[c]CNC obtained was in sodium sulfate form.
[d]TOCN was in sodium carboxylate form.

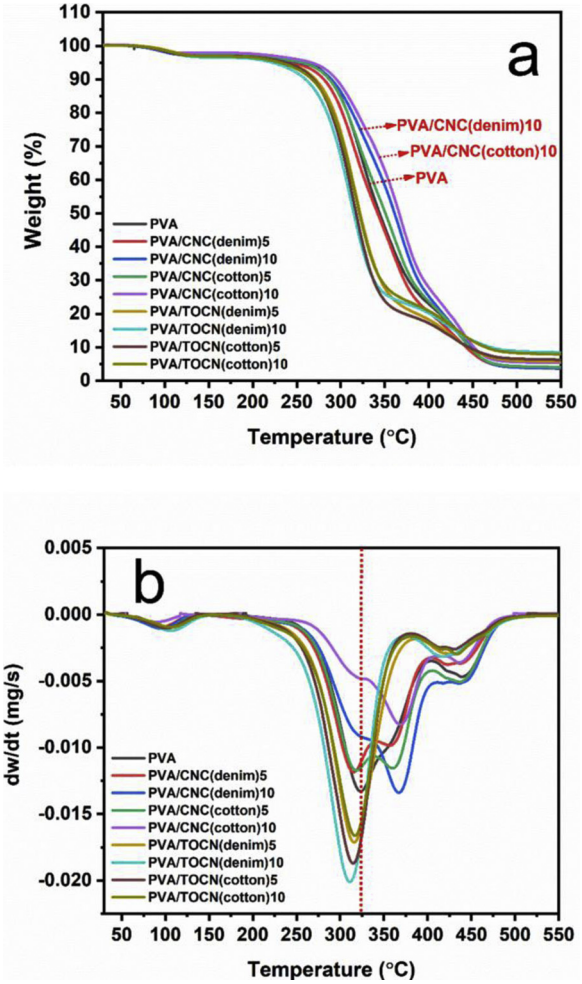

Fig. 6. TGA curve (a) and DTG curves (b) of the PVA composites with different types of nanocellulose at various concentrations (0%, 5%, and 10 %).

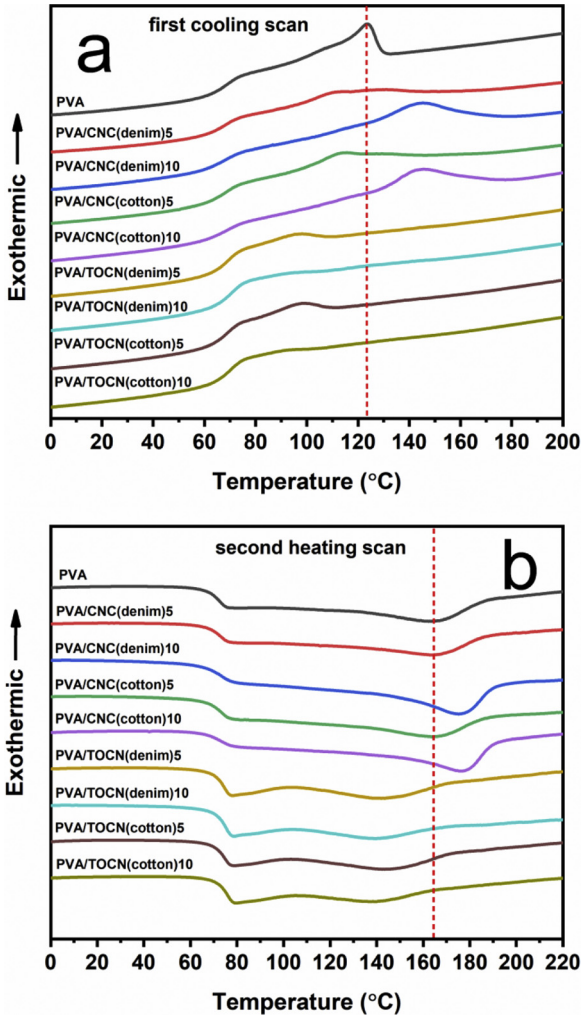

Fig. 7. DSC thermograms of the first cooling scan (a) and the second heating scan (b) of the PVA composites with different types of nanocellulose at various concentrations (0%, 5%, and 10 %).

peaks at around 250 ℃ and 300 ℃corresponding to the degradation of the sodium anhydroglucuronate units and the degradation of crystalline cellulose chain (Fukuzumi et al., 2010). The TEMPO oxidation had a more pronounced influence on the thermal properties than the strong acid hydrolysis due to the introduction of carboxyl groups during the TEMPO-oxidation process (Fukuzumi et al., 2010). As presented in Table 2 and Fig. 4, overall, cotton-sourced nanocellulose (CNC or TOCN) had relatively higher onset degradation temperature and the maximum degradation temperature as comparison to those derived from the wood source, showing cotton-sourced nanocellulose had slightly higher thermal stability.

3.4. Tensile properties of cotton-sourced nanocellulose reinforced PVA composites

Fig. 5 shows the tensile strength and tensile modulus of PVA composite films prepared with CNCs and TOCNs at 5% and 10 % loadings. Except for the addition of 10 % CNC(indigo-dyed denim) which resulted in decreased tensile strength (Fig. 5a) when compared to the pure PVA film, all the other formulations showed a reinforcing effect. Films made with 5% CNC(indigo-dyed denim) were stronger than the pure PVA film. The decrease in tensile strength of 10 % CNC(indigo-dyed denim) filled film might be resulted from the poor PVA-indigo interfacial bonding due to their opposite hydrophilicity. Indigo molecules bore hydrophobic aromatic moieties and there would be no strong interfacial bonding between these aromatic moieties and PVA. Therefore, weak spots existed in the CNC(indigo-dyed denim) reinforced films. The water contact angle results shown in Fig. S1 confirmed that films made with CNC(indigo-dyed) were more hydrophobic (with higher water contact angle) than films made with CNC(bleached cotton). When the CNC loading reached 10 %, the reduced tensile strength caused by these weak spots surpassed the increased strength brought by CNC reinforcing. TOCN(indigo-dyed denim) containing no denim dyes showed good reinforcing effects at 10 % loading. In terms of tensile modulus, it has been well-known that nanocellulose can provide plastic composites with improved modulus because of the incorporation of stiff crystals or nanofibers to form a rigid network within the matrix (Iwatake, Nogi, & Yano, 2008; Lee, Aitomäki, Berglund, Oksman, & Bismarck, 2014). As can be seen in Fig. 5b, the incorporation of nanocellulose in both bleached cotton and indigo-dyed denim resulted in increased tensile modulus as expected. The higher the nanocellulose content, the larger the modulus, in general, with the only exception of CNC(indigo-dyed denim) filled PVA films. From 5%–10% of CNC(indigo-dyed denim), the film modulus dropped. This might be ascribed to the same reason as for the dropping of tensile strength discussed above, *i.e.,* weak PVA-dye interface (Klemm et al., 2011).

3.5. Thermal behaviors of cotton-sourced nanocellulose reinforced PVA composites

Although the incorporation of 10 % CNC(indigo-dyed denim) into the PVA matrix resulted in tensile strength reduction, it is interesting to

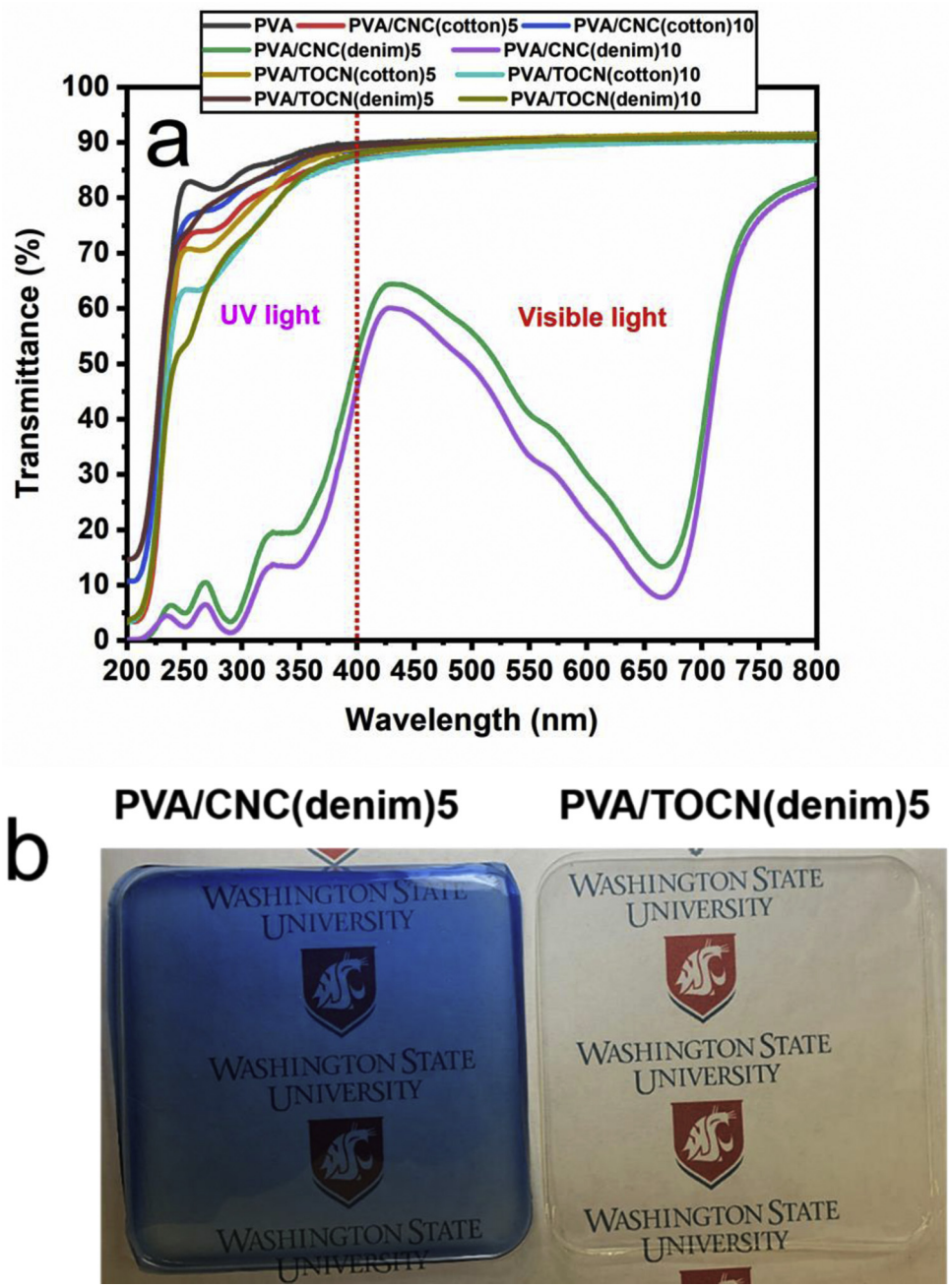

Fig. 8. (a) UV–vis spectra of PVA composites incorporated with different types of nanocellulose at different concentrations (0%, 5%, and 10 %); (b) Photograph of transparent PVA/CNC (denim)5 and PVA/TOCN (denim)5.

note from the TGA curves that their thermal stability improved. Both the onset (Fig. 6a) and the maximum degradation temperatures (Fig. 6b) shifted to the higher side. A similar improved thermal stability was observed in the PVA composites with 10 % CNC(bleached cotton). In contrast, the addition of TOCN was detrimental to the thermal stability of the PVA composites. This might be attributed to the significantly deteriorated thermal stability of TOCN during TEMPO oxidation, as discussed in section 3.3.

The influence of nanocellulose on non-isothermal crystallization and melting behavior of the PVA composites was investigated with DSC. The thermal history of the composites was eliminated during the first heating scan to 250 °C. Upon cooling and reheating, the films containing CNC and TOCN showed different crystallization behaviors. The different concentration of TOCN did not have much influence on the overall behavior of the PVA/TOCN films; in contrast, the concentrations of CNC at 5% and 10 % did show distinct effects. In the first cooling scan (Fig. 7a), the exothermic peak resulted from crystallization of the pure PVA occurred at around 125 °C. With 5% CNC (from both denim and white cotton), the magnitude of the exothermic peaks significantly decreased and crystallization started with a lower onset temperature. When the CNC concentration increased to 10 %, the exothermic peaks were more evident with higher onset temperature (140 °C) than that of pure PVA. This indicated an enhanced crystallization ability of PVA as a result of the nucleation effect of CNC at a higher loading (Pei, Zhou, & Berglund, 2010; Suryanegara, Nakagaito, & Yano, 2009). Nucleation and chain confinement are two competing factors affecting crystallization and crystallinity of polymers; their contribution can vary depending on the nanocellulose concentration (Ten, Bahr, Li, Jiang, & Wolcott, 2012). Higher CNC loading in the PVA matrix led to more interfacial areas and more nucleation sites for the improved

crystallization capability of PVA. Compared to CNC, TOCN was much longer in size. Therefore, the chain confinement effect of TOCN on PVA crystallization outweighed the nucleation effect as the results showed. PVA films containing TOCN, regardless of the concentration and the source of TOCN, exhibited broader exothermic peaks started from relatively lower temperatures.

In the second heating scan (Fig. 7b), the glass transition temperature was observed at around 75 ℃ for the pure PVA, a broad endothermic peak, corresponding to the melting of the crystalline phase of PVA, occurred at approximately 165 ℃. The glass transition temperature did not change considerably with the incorporation of nanocellulose (both CNC and TOCN). But the evident melting peak shifted to a higher temperature for the PVA composites containing 10 % CNC from both denim and bleached cotton. The PVA/TOCN composites did not exhibit evident endothermic peaks (crystal melting peaks), and this was in line with the results from the first cooling process.

3.6. Light transmission of cotton-sourced nanocellulose reinforced PVA composites

Fig. 8a shows light transmittance of the pure PVA and nanocellulose containing films. The addition of TOCN extracted from both the bleached cotton and denim and CNC from the bleached cotton did not affect the film clarity as the transmittance in the visible light range kept at 90 %, same as pure PVA films. Films containing blue CNC from denim blocked the light with a wavelength at around 675 nm due to the absorption of indigo dyes. Nevertheless, the film still kept its transparency as shown in Fig. 8b. At lower wavelengths, the films blocked 83.5 % and 89.2 % of UV light in the range of 200 − 400 nm when 5% and 10 % of CNC(indigo-dyed denim) were added, respectively. The UV absorption was much larger than the neat PVA film, which had 27 % UV blocking. The resonance of the aromatic ring, the carboxyl groups, and the amino groups in indigo molecule absorbed UV light at the wavelength of 205 nm, 250 nm, and 290 nm (Ortiz et al., 2016). These results indicated that the CNC(indigo-dyed denim) reinforced PVA films would have great potential for food packaging applications because of the blue color, the improved strength and modulus, as well as the enhanced UV blocking.

4. Conclusions

Sulfuric acid hydrolysis and TEMPO-oxidation methods were applied to extract nanocellulose from indigo-dyed denim fabric, bleached cotton fabric, and wood pulp, aiming to examine the influence of indigo dyes on nanocellulose extraction and the ensuing nanocellulose characteristics for the potential of recycling denim waste for nanocellulose. The results showed that indigo dyes on the cellulose had little influence on the nanocellulose extraction and their material properties in terms of yield, morphology, size, surface charge, crystallinity, and thermal properties when compared to those from bleached cotton. The TEMPO-oxidation method not only oxidized cellulose but also degraded indigo dyes simultaneously during the process. Sulfuric acid hydrolysis could not degrade indigo dyes and the stable blue-color suspension was produced. Compared to wood pulp, cotton yielded nanocellulose with a higher cellulose crystallinity and thermal stability. The CNC and TOCN extracted from indigo-dyed denim and bleached cotton exhibited their reinforcing effects in the PVA matrix at both 5% and 10 % nanocellulose loading with the only exception of 10 % CNC(indigo-dyed denim). However, the 10 % CNC(indigo-dyed denim) or CNC(bleached cotton) addition was found to improve the thermal stability of the PVA composites as well as enhancing the crystallizability of PVA. The addition of indigo-dyed CNC was also found to reduce the transmittance of UV light through PVA composites. The results suggested that indigo-dyed denim fabric could be used as a starting material for nanocellulose production and the nanocellulose produced had great potential as a multi-functional filler to provide composites with blue color, improved tensile properties, and UV-resistance properties.

CRediT authorship contribution statement

Tuhua Zhong: Conceptualization, Methodology, Investigation, Writing - original draft. **Renuka Dhandapani:** Methodology, Writing - review & editing. **Dan Liang:** Investigation. **Jinwu Wang:** Conceptualization, Methodology, Writing - review & editing, Funding acquisition. **Michael P. Wolcott:** Conceptualization, Methodology, Writing - review & editing, Funding acquisition. **Dana Van Fossen:** Investigation. **Hang Liu:** Conceptualization, Methodology, Writing - review & editing, Supervision, Funding acquisition.

Declaration of Competing Interest

None.

Acknowledgements

This work was supported by Cotton Incorporated, USA (Award No. 19-888).

Appendix A. Supplementary data

Supplementary material related to this article can be found, in the online version, at doi:https://doi.org/10.1016/j.carbpol.2020.116283.

References

Baran, A., Fiedler, A., Schulz, H., & Baranska, M. (2010). In situ Raman and IR spectroscopic analysis of indigo dye. *Analytical Methods, 2*(9), 1372–1376. https://doi.org/10.1039/c0ay00311e.

Bechtold, T., Maier, P., & Schrott, W. (2005). Bleaching of indigo-dyed denim fabric by electrochemical formation of hypohalogenites in situ. *Coloration Technology, 121*(2), 64–68. https://doi.org/10.1111/j.1478-4408.2005.tb00252.x.

Beck-Candanedo, S., Roman, M., & Gray, D. G. (2005). Effect of reaction conditions on the properties and behavior of wood cellulose nanocrystal suspensions. *Biomacromolecules, 6*(2), 1048–1054. https://doi.org/10.1021/bm049300p.

Brinchi, L., Cotana, F., Fortunati, E., & Kenny, J. M. (2013). Production of nanocrystalline cellulose from lignocellulosic biomass: Technology and applications. *Carbohydrate Polymers, 94*(1), 154–169. https://doi.org/10.1016/j.carbpol.2013.01.033.

de Assis, C. A., Houtman, C., Phillips, R., Bilek, E. M., Rojas, O. J., Pal, L., ... Gonzalez, R. (2017). Conversion ecibinucs if forest biomaterials: Risk and financial analysis of CNC manufacturing. *Biofuels Bioproducts and Biorefining, 11*, 682–700. https://doi.org/10.1002/bbb.

Dong, X. M., Revol, J., & Gray, D. G. (1998). Effect of microcrystallite preparation conditions on the formation of colloid crystals of cellulose. *Cellulose, 5*, 19–32.

Dufresne, A. (2013). Nanocellulose: A new ageless bionanomaterial. *Materials Today, 16*(6), 220–227. https://doi.org/10.1016/j.mattod.2013.06.004.

EI Mogahzy, Y. E. (2009). *Engineering textile-integrating the design and manufacture of textile products* (1st ed.). Cambridge: Woodhead Publishing Chapter 12.

Foster, E. J., Moon, R. J., Agarwal, U. P., Bortner, M. J., Bras, J., Camarero-Espinosa, S., ... Youngblood, J. (2018). Current characterization methods for cellulose nanomaterials. *Chemical Society Reviews, 47*(8), 2609–2679. https://doi.org/10.1039/c6cs00895j.

French, A. D. (2014). Idealized powder diffraction patterns for cellulose polymorphs. *Cellulose, 21*(2), 885–896. https://doi.org/10.1007/s10570-013-0030-4.

French, A. D., & Cintrón, M. S. (2013). Cellulose polymorphy, crystallite size, and the Segal crystallinity index. *Cellulose, 20*(1), 583–588. https://doi.org/10.1007/s10570-012-9833-y.

Fukuzumi, H., Saito, T., Okita, Y., & Isogai, A. (2010). Thermal stabilization of TEMPO-oxidized cellulose. *Polymer Degradation and Stability, 95*(9), 1502–1508. https://doi.org/10.1016/j.polymdegradstab.2010.06.015.

Habibi, Y., Lucia, L. A., & Rojas, O. J. (2010). Cellulose nanocrystals: Chemistry, self-assembly, and applications. *Chemical Reviews, 110*(6), 3479–3500. https://doi.org/10.1021/cr900339w.

Hamad, W. (2006). On the development and applications of cellulosic nanofibrillar and nanocrystalline materials. *The Canadian Journal of Chemical Engineering, 84*, 513–519.

Hamad, W. Y., & Hu, T. Q. (2010). Structure-process-yield interrelations in nanocrystalline cellulose extraction. *The Canadian Journal of Chemical Engineering, 88*(3), 392–402. https://doi.org/10.1002/cjce.20298.

Haule, L. V., Carr, C. M., & Rigout, M. (2016). Preparation and physical properties of regenerated cellulose fibres from cotton waste garments. *Journal of Cleaner Production, 112*, 4445–4451. https://doi.org/10.1016/j.jclepro.2015.08.086.

Helbert, W., Nishiyama, Y., Okano, T., & Sugiyama, J. (1998). Molecular imaging of Halocynthia papillosa cellulose. *Journal of Structural Biology, 124*, 42–50. https://doi.org/10.1006/jsbi.1998.4045.

Isogai, A., Saito, T., & Fukuzumi, H. (2011). TEMPO-oxidized cellulose nanofibers. *Nanoscale, 3*(1), 71–85. https://doi.org/10.1039/c0nr00583e.

Iwatake, A., Nogi, M., & Yano, H. (2008). Cellulose nanofiber-reinforced polylactic acid. *Composites Science and Technology, 68*, 2103–2106. https://doi.org/10.1016/j.compscitech.2008.03.006.

Jiang, F., & Hsieh, Y. L. (2015). Cellulose nanocrystal isolation from tomato peels and assembled nanofibers. *Carbohydrate Polymers, 122*, 60–68. https://doi.org/10.1016/j.carbpol.2014.12.064.

Jordan, J. H., Easson, M. W., Dien, B., Thompson, S., & Condon, B. D. (2019). Extraction and characterization of nanocellulose crystals from cotton gin motes and cotton gin waste. *Cellulose, 26*(10), 5959–5979. https://doi.org/10.1007/s10570-019-02533-7.

Kim, D. Y., Nishiyama, Y., Wada, M., & Kuga, S. (2001). High-yield carbonization of cellulose by sulfuric acid impregnation. *Cellulose, 8*(1), 29–33. https://doi.org/10.1023/A:1016621103245.

Klemm, D., Kramer, F., Moritz, S., Lindström, T., Ankerfors, M., Gray, D., ... Dorris, A. (2011). Nanocelluloses: A new family of nature-based materials. *Angewandte Chemie - International Edition, 50*(24), 5438–5466. https://doi.org/10.1002/anie.201001273.

Lakshmi, U. R., Srivastava, V. C., Mall, I. D., & Lataye, D. H. (2009). Rice husk ash as an effective adsorbent: Evaluation of adsorptive characteristics for Indigo Carmine dye. *Journal of Environmental Management, 90*(2), 710–720. https://doi.org/10.1016/j.jenvman.2008.01.002.

Lee, K. Y., Aitomäki, Y., Berglund, L. A., Oksman, K., & Bismarck, A. (2014). On the use of nanocellulose as reinforcement in polymer matrix composites. *Composites Science and Technology, 105*, 15–27. https://doi.org/10.1016/j.compscitech.2014.08.032.

Lin, N., & Dufresne, A. (2014). Surface chemistry, morphological analysis and properties of cellulose nanocrystals with gradiented sulfation degrees. *Nanoscale, 6*(10), 5384–5393. https://doi.org/10.1039/c3nr06761k.

Liu, W., Liu, S., Liu, T., Liu, T., Zhang, J., & Liu, H. (2019). Eco-friendly post-consumer cotton waste recycling for regenerated cellulose fibers. *Carbohydrate Polymers, 206*, 141–148. https://doi.org/10.1016/j.carbpol.2018.10.046.

Maryan, A. S., & Montazer, M. (2013). A cleaner production of denim garment using one step treatment with amylase/cellulase/laccase. *Journal of Cleaner Production, 57*, 320–326. https://doi.org/10.1016/j.jclepro.2013.05.041.

Moon, R. J., Martini, A., Nairn, J., Simonsen, J., & Youngblood, J. (2011). Cellulose nanomaterials review: Structure, properties and nanocomposites. *Chemical Society Reviews, 40*. https://doi.org/10.1039/c0cs00108b.

Morais, J. P., de Freitas Rosa, M., Nascimento, L. D., do Nascimento, D. M., & Cassales, A. R. (2013). Extraction and characterization of nanocellulose structures from raw cotton linter. *Carbohydrate polymers, 91*(1), 229–235. https://doi.org/10.1016/j.carbpol.2012.08.010.

Ortiz, E., Gómez-Chávez, V., Cortés-Romero, C. M., Solís, H., Ruiz-Ramos, R., & Loera-Serna, S. (2016). Degradation of indigo carmine using advanced oxidation processes: Synergy effects and toxicological study. *Journal of Environmental Protection, 07*(12), 1693–1706. https://doi.org/10.4236/jep.2016.712137.

Pedersoli Júnior, J. L. (2000). Effect of cellulose crystallinity on the progress of thermal oxidative degradation of paper. *Journal of Applied Polymer Science, 78*, 61–66.

Pei, A., Zhou, Q., & Berglund, L. A. (2010). Functionalized cellulose nanocrystals as biobaed nucleation agents in poly(L-lactide) (PLLA)-Crystallization and mechanical property effects. *Composites Science and Technology, 70*, 815–821.

Rebouillat, S., & Pla, F. (2013). State of the art manufacturing and engineering of nanocellulose: A review of available data and industrial applications. *Journal of Biomaterials and Nanobiotechnology, 04*(02), 165–188. https://doi.org/10.4236/jbnb.2013.42022.

Reid, M. S., Villalobos, M., & Cranston, E. D. (2017). Benchmarking cellulose nanocrystals: From the laboratory to industrial production. *Langmuir, 33*(7), 1583–1598. https://doi.org/10.1021/acs.langmuir.6b03765.

Roman, M., & Winter, W. T. (2004). Effect of sulfate groups from sulfuric acid hydrolysis on the thermal degradation behavior of bacterial cellulose. *Biomacromolecules, 5*(5), 1671–1677. https://doi.org/10.1021/bm034519+.

Saito, T., & Isogai, A. (2004). TEMPO-mediated oxidation of native cellulose. The effect of oxidation conditions on chemical and crystal structures of the water-insoluble fractions. *Biomacromolecules, 5*(5), 1983–1989. https://doi.org/10.1021/bm0497769.

Saito, T., Nishiyama, Y., Putaux, J., Vignon, M., & Isogai, A. (2006). Homogeneous suspensions of individualized microfibrils from TEMPO-catalyzed oxidation of native cellulose. *Biomacromolecules, 7*(6), 1687–1691.

Segal, L., Creely, J. J., Martin, A. E., & Conrad, C. M. (1959). An empirical emthod for estimating the degree of crystallinity of native cellulose using the X-ray diffractometer. *Textile Research Journal, 29*(10), 786–794. https://doi.org/10.1002/bit.

Shamskar, K. R., Heidari, H., & Rashidi, A. (2016). Preparation and evaluation of nanocrystalline cellulose aerogels from raw cotton and cotton stalk. *Industrial Crops and Products, 93*, 203–211. https://doi.org/10.1016/j.indcrop.2016.01.044.

Soni, B., & Mahmoud, B. (2015). Chemical isolation and characterization of different cellulose nanofibers from cotton stalks. *Carbohydrate polymers, 134*, 581–589. https://doi.org/10.1016/j.carbpol.2015.08.031.

Suryanegara, L., Nakagaito, A. N., & Yano, H. (2009). The effect of crystallization of PLA on the thermal and mechanical properties of microfibrillated cellulose-reinforced PLA composites. *Composites Science and Technology, 69*, 1187–1192.

Ten, E., Bahr, D. F., Li, B., Jiang, L., & Wolcott, M. P. (2012). Effects of cellulose nanowhiskers on mechancial dielectric and rheological properties of poly(3-hydroxybutyrate-co-3-hydroxyvalerate)/cellulose nanowhisker composites. *Industrial & Engineering Chemistry Research, 51*, 2941–2951.

Teixeira, E. de Morais, Corrêa, A. C., Manzoli, A., de Lima Leite, F., de Oliveira, C. R., & Mattoso, L. H. (2016). Cellulose nanofibers from white and naturally colored cotton fibers. *Cellulose, 17*(3), 595–606. https://doi.org/10.1007/s10570-010-9403-0.

Vanderfleet, O. M., Reid, M. S., Bras, J., Heux, L., Godoy-Vargas, J., Panga, M. K. R., ... Cranston, E. D. (2019). Insight into thermal stability of cellulose nanocrystals from new hydrosis methods with acid blends. *Cellulose, 26*, 507–528.

Wada, M., Heux, L., & Sugiyama, J. (2004). Polymorphism of cellulose I family: Reinvestigation of cellulose IVl. *Biomacromolecules, 5*(4), 1385–1391. https://doi.org/10.1021/bm0345357.

Wambuguh, D., & Chianelli, R. R. (2008). Indigo dye waste recovery from blue denim textile effluent: A by-product synergy approach. *New Journal of Chemistry, 32*(12), 2189–2194. https://doi.org/10.1039/b806213g.

Wang, Z., Yao, Z. J., Zhou, J., & Zhang, Y. (2017). Reuse of waste cotton cloth for the extraction of cellulose nanocrystals. *Carbohydrate Polymers, 157*, 945–952. https://doi.org/10.1016/j.carbpol.2016.10.044.